Kinetically Controlled Growth and Shape Formation Mechanism of Platinum Nanoparticles

Janet M. Petroski,[†] Zhong L. Wang,[‡] Travis C. Green,[†] and Mostafa A. El-Sayed*,[†]

Laser Dynamics Laboratory, School of Chemistry and Biochemistry, Georgia Institute of Technology, Atlanta, Georgia 30332-0400, and School of Materials Science and Engineering, Georgia Institute of Technology, Atlanta, Georgia 30332-0245

Recently, we have been able to synthesize platinum colloidal nanoparticles of different shapes (*Science*, **1996,** *272,* 1924). In this report, we present transmission electron microscopic (TEM) results on the time-dependent shape distribution of platinum nanoparticles during the growth period and its dependence on the concentration of the capping polymer as well as the pH of the solution. The results suggest a shape-controlled growth mechanism in which the difference between the rate of the catalytic reduction process of Pt^{2+} on the {111} and {100} faces, the competition between the Pt^{2+} reduction and the capping process on the different nanoparticle surfaces, and the concentration-dependent buffer action of the polymer itself all control the final distribution of the different shapes observed.

Introduction

Colloidal metal nanoparticles are of great interest because of their use as catalysts,[1] photocatalysts,[2] adsorbents and sensors,[3] and ferrofluids[4] and because of their applications in optical,[5] electronic,[5] and magnetic devices.[3] Many studies on colloidal nanoparticles have focused on the control of nanoparticle sizes and their growth kinetics and have correlated nanoparticle size to the catalytic activity.[6] Recently, our group has reported[7] for the first time a technique that controlled the shape distribution of Pt nanoparticles. This was accomplished by changing the ratio of the concentration of the capping polymer material to that of the platinum cations used in the reductive synthesis of colloidal nanoparticles in solution at room temperature. Cubic, tetrahedral, and truncated octahedral (TO) nanoparticles have been prepared in high percentages, thus making it possible to study the catalytic activities of nanoparticles with different shapes and crystal facets.[8]

From theoretical considerations,[9] clusters with {111} faces such as those present in tetrahedral or TO nanoparticles should be the most stable. Previously, the formation of a greater abundance of cubic nanoparticles with their less stable {100} faces was achieved.[7] This result compelled us to study the details of the growth mechanism for the shape-controlled processes of Pt nanoparticles. A recent publication discussed[10] the previously proposed growth mechanisms (both thermodynamically and kinetically controlled) and suggested a general kinetically controlled one for nanocluster growth, but without shape-controlled considerations, using the H_2 reduction method (see Note Added in Proof).

Using transmission electron microscopy (TEM), we imaged the shapes and determined the shape distribution of platinum nanoparticles at different stages of their growth as a function of time. The small nanoparticles formed during the early stages of growth or at high polymer concentration displayed distributions with a dominance of shapes having the stable {111} faces.

As the growth continues or at low polymer to Pt complex concentration ratio, *the tetrahedral nanoparticles are transformed into TO and eventually into cubic shapes.* A mechanism is proposed in which the initially rapid reduction of Pt^{2+} produces an initial growth that gives very small nanoparticles having the expected stable {111} faces present in tetrahedra and TO. The competition between polymer capping and H_2 reduction of the Pt^{2+} complex *occurring on the most catalytically active {111} surface*[11] determines the fate of these tetrahedral nanoparticles. If capping dominates, tetrahedral nanoparticles of small size are formed. Otherwise, the rapid reduction of the Pt^{2+} on the most active {111} surface leads to its disappearance and the formation of a {100} face due to the deposition of Pt atoms on it to give larger TO nanoparticles having both {100} and {111} faces. The TO nanoparticles continue to grow until transformed into cubic nanoparticles, which have all of their six faces of the {100} type. We also found that the polymer, acting both as a capping molecule and as a buffering agent, plays an important role in this competition.

Experimental Section

Pt nanoparticles were prepared by using the technique of Rampino and Nord[12] and Henglein et al.[13] by bubbling Ar gas through the aged solution of K_2PtCl_4 which was adjusted to an initial pH of ∼7 and reduced by flowing H_2 gas through the solution. The starting ratio of K_2PtCl_4 to polyacrylate (M_W 2100) was either 1:1 (low polymer concentration) or 1:5 (high polymer concentration) with the initial concentration of K_2PtCl_4 being 8×10^{-5} M. The TEM grids were prepared for imaging by placing a small drop of the specimen solution on a copper grid having an amorphous carbon film less than 20 nm thick and allowing it to dry completely in air at ambient temperature. A time sequence of specimens was collected the first hour and then every 2 h starting from the time when the H_2 flow was stopped until growth ceased to examine the time profile of the shape distribution of the nanoparticles. The end point of the nanoparticle growth was ascertained when there was no longer changes in the pH reading and the absorption spectrum. The pH was measured at the moment when the specimen was

* To whom correspondence should be addressed.
† School of Chemistry and Biochemistry.
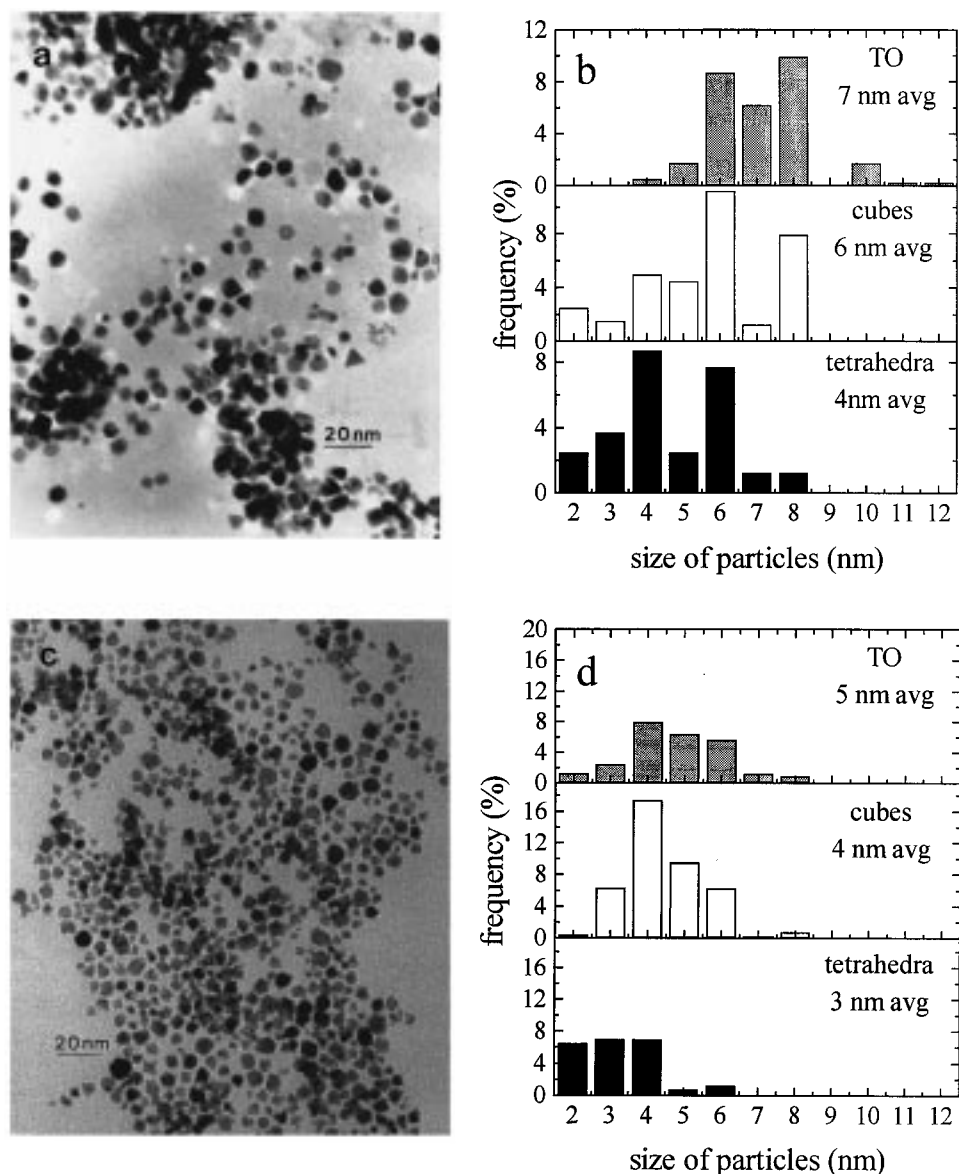‡ School of Materials Science and Engineering.

Letters

J. Phys. Chem. B, Vol. 102, No. 18, 1998 **3317**

Figure 1. (a) TEM images of Pt nanoparticles grown in a low polymer concentration solution and collected at $t = 1$ h after the flow of H_2. (b) The size and shape distribution for the TEM image shown in Figure 1a for the cubic, tetrahedral, and truncated octahedral (TO) nanoparticles. The average size of each shape (determined from the center of a Gaussian distribution) is indicated at the right of the distribution. The percentage of unidentified (shapeless) nanoparticles is not included in the distribution figures. This figure shows that the smallest nanoparticle shape is tetrahedra while the largest shape is TO. (c) TEM image of Pt nanoparticles grown in a high polymer concentration solution and collected at $t = 1$ h after the flow of H_2. (d) The size and shape distribution for the TEM image shown in Figure 1c for the cubic, tetrahedral, and truncated octahedral (TO) nanoparticles. The average size of each shape (determined from the center of a Gaussian distribution) is indicated to the right of the distribution. This figure shows a similar distribution as Figure 1b, but the average sizes are smaller, thereby indicating a more efficient capping process owing to the higher polymer concentration.

collected. The nanoparticle shapes were determined at 200 kV using a Hitachi HF-2000 TEM equipped with a field emission source.

Results and Discussion

Figure 1a shows a low-magnification TEM image, and Figure 1b shows the nanoparticle size distribution of the different shapes for nanoparticles grown from an initial 1:1 concentration ratio collected at $t = 1$ h. The distribution measures the size of each nanoparticle shape present in the TEM image that consisted of over 400 nanoparticles. The average size of each nanoparticle is indicated in the figure and was calculated from the center of a Gaussian distribution. Parts c and d of Figure 1 show similar results to those in parts a and b, respectively, for a sample prepared from initial ratio of 1:5 also at $t = 1$ h, found from counting over 630 nanoparticles. From these

figures, it can be seen that nucleation is already complete and growth has commenced in less than 1 h. Also, the smallest shape in both figures is tetrahedral, but the average size of each shape is larger in the 1:1 ratio, as shown in Figure 1b, d. This indicates faster growth in the sample grown from the 1:1 ratio.

Figure 2a gives the time-dependent percentages of the different shapes of nanoparticles present in a system synthesized with a 1:1 initial ratio of K_2PtCl_4 to polymer concentration (determined from the TEM images in a manner similar to that used to obtain Figure 1). The total number of nanoparticles counted in this figure was 4190 with an average number of $\sim$ 450 nanoparticles for each specimen's TEM image (a sample of one of the first hour's image is shown in Figure 1). At least one, but sometimes two, image was counted for each time period. These are represented by the additional set of shapes found at that time in the figure. The unidentified nanoparticles
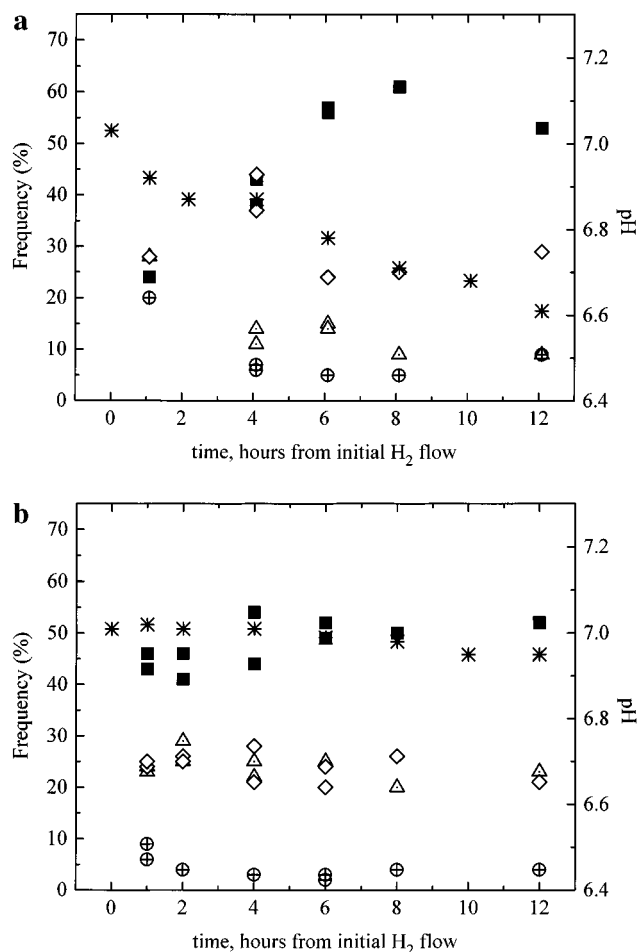
Figure 2. (a) Time dependence of the shape distribution of the different Pt nanoparticles collected from images containing a much larger number of nanoparticles than those shown in Figure 1a, b for a 1:1 Pt^{2+} to polyacrylate ratio and (b) for a 1:5 ratio. The changes in the percentages of cubic (■), tetrahedral (△), truncated octahedral (◇), and unidentified (⊕) nanoparticles are shown, as well as the change in the pH (*) over the same time period. This figure shows that at low polymer concentration (a), cubes are formed at the expense of the tetrahedra as the pH decreases with time, while at high polymer concentration (b), the distribution as well as the pH remain independent of time.

refer to those that are oriented irregularly on the carbon film support so that their shapes cannot be directly identified in TEM images.

From the distribution and the TEM images shown in Figures 1 and 2a, four main features are seen. First, the average nanoparticle size increases from ~5 to ~10 nm in 12 h after stopping the H_2 flow. The second feature is the strong dependence on time of the relative percentages of cubic, tetrahedral, and TO nanoparticles in the solution. The percentage of cubes increases with time, while the percentage of tetrahedra decreases. The percentage of TO, however, increases first then decreases slightly. Third, the dominant shape at $t = 1$ h is tetrahedral and TO, while the dominant one at $t = 12$ h is cubic. Finally, it is important to notice in Figure 2a that the pH decreases from 7.03 at $t = 0$ h to 6.61 at $t = 12$ h during the growth period.

Figure 2b gives the results of Pt nanoparticles grown in a solution in which the initial concentration of K_2PtCl_4 to the polymer is in a 1:5 ratio (determined from the TEM images in a manner similar to that used to obtain Figure 1). The total number of nanoparticles counted in this figure was 4152 with an average number of ~425 nanoparticles for each specimen's TEM image (a sample of one of the first hour's images is shown
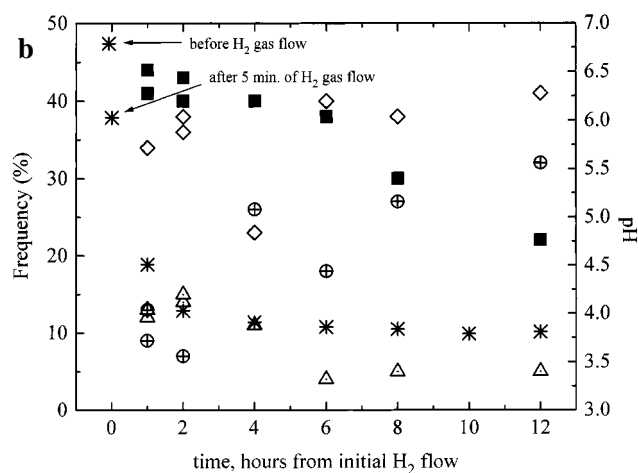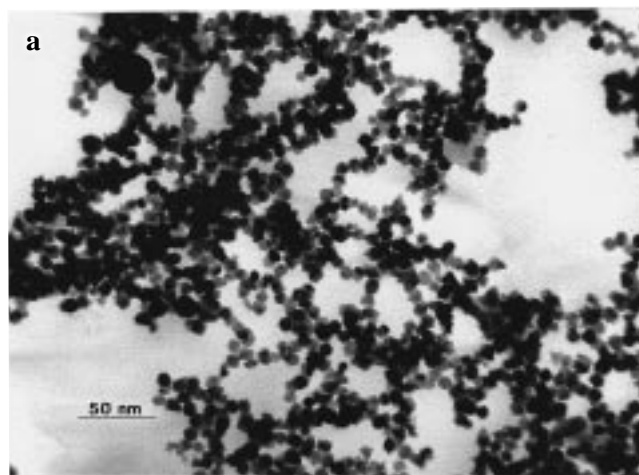
Figure 3. (a) TEM image of the Pt nanoparticles grown without the addition of the polyacrylate capping material and collected at $t = 12$ h after the flow of H_2. (b) Time dependence of the shape distribution of Pt nanoparticles grown without polyacrylate in a solution of initial pH $= 6.79$ before bubbling the H_2 gas into the solution. The changes in the percentages of cubic (■), tetrahedral (△), truncated octahedral (◇), and unidentified (⊕) nanoparticles are shown, as well as the change in the pH (*) over the same time period. Note that the pH changes to 6.03 after only 5 min of H_2 gas flow which shows the rapid initial appearance of the H^+ signifying a corresponding initial rapid formation of Pt atoms leading to the nucleation process. This figure also shows the instability of the shapes of these nanoparticles when it is uncapped as the percentage of the unidentified shapes (⊕) increases with time. (The unidentified nanoparticles refer to those that are oriented irregularly on the carbon film support so that their shapes cannot be directly identified in the TEM images.)

in Figure 1). Sometimes an additional image was counted and shown as an additional set of shapes in the figure. A different time-dependent shape distribution and pH profile are observed from that shown in Figure 2a. Unlike the 1:1 ratio results above, the relative percentages of cubes, tetrahedra, and truncated octahedra remain almost independent of the growth time, but the average nanoparticle size increases from ~4 to ~8 nm in 12 h after stopping the H_2 flow. The pH of the solution also remains relatively constant with time.

To measure the rate of reduction of Pt^{2+} into Pt, the rate of appearance of the H^+ ion produced from H_2 was monitored in the absence of the buffer action of the polyacrylate. A portion of a low-magnification TEM image of these "uncapped" nanoparticles grown after 12 h is shown in Figure 3a. Figure 3b shows the time dependence of both nanoparticle growth and the pH of the solution in the absence of the capping polymer. In this figure, the total number of nanoparticles counted was

Letters

J. Phys. Chem. B, Vol. 102, No. 18, 1998 **3319**

5745 with an average of ∼575 nanoparticles per TEM image. Sometimes an additional image was counted and shown as an additional set of shapes in the figure. Over the first hour, the $[H_3O^+]$ increases by more than 2 orders of magnitude to a value of 5×10^{-5} M. Therefore, approximately 50% of the Pt ions have been reduced during this time. The nucleation and growth give rise to cubes and TO but very little tetrahedra. This suggests that the capping polymer is needed for the initial formation of large amounts of tetrahedra. Figure 3b also shows that as the growth continues, more and more of the cubes and TO are transformed into larger shapeless (unidentified) nanoparticles in the absence of a stabilizer. Unlike the more stable nanoparticles grown with the polyacrylate, these nanoparticles aggregate until they precipitate out of solution.

One can summarize the important results as follows: (1) Almost half of the initially used Pt^{2+} ions are reduced in a short period of time allowing for rapid reduction and the formation of the initial nuclei. (The pH change is 6.79 to 6.03 in 5 min after introducing H_2 in the absence of the polymer. One expects similar initial rates in the presence of the polymer; however, owing to its buffering action, only slight changes in the pH occur in the 1:1 mixture (7.08 to 7.03) and no change was observed in the 1:5 solution for the same time period of 5 min.). (2) The average size of the tetrahedral nanoparticles (which are observed in the presence of capping polymer) is always smaller than that of the cubic or TO nanoparticles. (3) During the growth process, the pH remains constant at high polymer concentration but continues to decrease at low polymer concentration. (4) In the early stages of growth, tetrahedral nanoparticles are present in significant quantities; in addition to this, at high polymer concentration, no observable interconversion between nanoparticle shapes takes place. (5) At low polymer (buffer) concentration conversion of tetrahedral nanoparticles into TO and then to larger cubic nanoparticles takes place as a result of the growth process.

The above results suggest the following mechanism: (1) rapid initial reduction leads to formation of stable nanoparticles with tetrahedral and TO shapes; (2) the growth process involves the H_2 reduction of the Pt^{2+} (in K_2PtCl_4 or in the hydrated form) to Pt atoms *on the surface of the Pt nanoparticles* formed initially in solution; (3) the reduction process is in competition with the surface capping process by the polymer; (4) the relative rates of the polymer capping, decapping (by the protonation of the polymer molecules on the capped small nanoparticles) and the relative reduction rates on the different surfaces (and thus the relative growth rates of the different faces, see Appendix) determine the final shape distribution.

The above mechanism is found to account for the observed results. Initially or at high polymer concentration, capping of the tetrahedral nanoparticles takes place and they are prevented from rapid growth leading to a distribution dominated with tetrahedral shapes. This accounts for the fact that tetrahedral nanoparticles are almost always smaller in size than those of the cubes and TO (result 2). During the growth period, the reduction of Pt^{2+} with the H_2 on the nanoparticle surface allows for nanoparticle growth and produces H^+ ions in solution. At high polymer concentration, the polymer not only caps the tetrahedral nanoparticle, but it also acts as a good buffer. This can be understood when one realizes that the capping polymer, which has a large number of carboxylate groups, acts as a good buffer if present in such high concentrations. Therefore, it does not allow for an increase in the $[H_3O^+]$ (see Figure 2b) and thus protects the capped tetrahedral nanoparticles from decapping. On the other hand, at low polymer concentration, the

buffer action is not strong, allowing for an increase in $[H_3O^+]$ in solution (result 3 as shown in Figure 2a). This is understood as more growth requires more Pt ions to be reduced by H_2, forming more H^+ with time if the buffer action of the polymer is not strong. This leads to the removal of the polymer from the surfaces of the capped tetrahedral nanoparticles, allowing for its further growth. Since the {111} face is more catalytically active,[11] the reduction of the Pt^{2+} into Pt atoms on this face converts tetrahedral and TO nanoparticles into the larger cubic nanoparticles (see Appendix) at low polymer concentration, in agreement with experimental observations (result 5). Therefore, as the growth process continues, more TO and cubic nanoparticles will be formed, while the percentage of the tetrahedral nanoparticles decreases (see Figure 2a).

Note Added in Proof: The proposed mechanism presented here was developed prior to our knowledge of the general mechanism proposed in ref 10. The two mechanisms share some general ideas.

Appendix

The growth of the four {111} planes transform a tetrahedral nanoparticle into a TO, which in turn can grow into a cubic nanoparticle (see b below). Therefore, as the growth process continues, more TO and cubic nanoparticles will be formed, while the percentage of the tetrahedral nanoparticles decreases, in agreement with the observation shown in Figure 2a. Small {111} corners can be left over if the system runs out of the Pt supply, as observed previously for cubic nanoparticles.[14]

On the basis of the fundamental face-centered cubic lattice of Pt, when the atoms are defined to be at the edges of the unit cell, the connection of all 13 atoms forms a TO shape cluster, which is bound by eight {111} and six {100} planes. If the growth rate (G) of the {111} plane ($G_{\{111\}}$) is significantly larger than that of the {100} ($G_{\{100\}}$), the {111} facets will vanish, forming a cubiclike nanoparticle. On the other hand, if $G_{\{100\}} \gg G_{\{111\}}$, the {100} facets will vanish, forming an octahedral nanoparticle. If $G_{\{100\}} \approx G_{\{111\}}$, the area ratio between the {111} and {100} facets remain constant, resulting in the formation of the larger TO nanoparticles. Thus the shape distribution at the end of the experiment is determined by the initial pH, the rate of reduction of Pt^{2+} ion on the different surfaces, and the rate of capping and decapping on the different surfaces (which depends on the changes in the pH during the growth).

a: Truncated Octahedron   b: Tetrahedron to TO and to cube
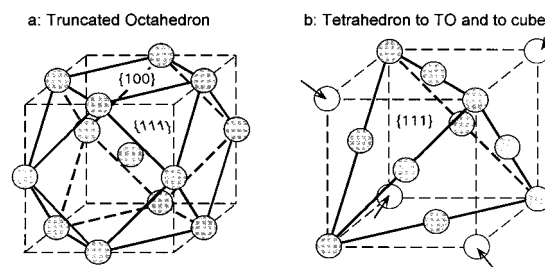
References and Notes

(1) Hirai, H.; Wakabayashi, H.; Komiyama, M. *Chem. Lett.* **1983**, *1983*, 1047.

(2) Brugger, P. A.; Cuendet, P.; Gratzel, M. *J. Am. Chem. Soc.* **1981**, *103*, 2923.

(3) Thomas, J. M. *Pure Appl. Chem.* **1988**, *60*, 1517.

(4) Charles, S. C.; Popplewell, J. In *Ferromagnetic Materials;* Wohlharth, E. P., Ed.; North-Holland: Amsterdam, 1980l Vol. 2.

(5) Schon, G.; Simon, U. *Colloid Polym. Sci.* **1995**, *273*, 202.

(6) Clint, J.H.,; et al. *Faraday Discuss. Chem. Soc.* **1993**, *95*, 219.

(7) (a) Ahmadi, T. S.; Wang, Z. L.; Green, T. C.; Henglein, A.; El-Sayed, M. A. *Science* **1996**, *272*, 1924. (b) Ahmadi, T. S.; Wang, Z. L.; Henglein, A.; El-Sayed, M. A. *Chem. Mater.* **1996**, *8*, 1161.

(8) Petroski, J. M.; Ahmadi, T. S.; El-Sayed, M. A.; Wang, Z. L., in preparation.

(9) Wales, D. J.; Kirkland, A. I.; Jefferson, D. A. *J. Chem. Phys.* **1989**, *91*, 603.

(10) Finke, R. G.; Watzky, M. A. *J. Am. Chem. Soc.* **1997**, *119*, 10382 and references therein.

(11) Falicov, L. M.; Somorjai, G. A. *Proc. Natl. Acad. Sci. U.S.A.* **1985**, *82*, 2207.

(12) Rampino, L. D.; Nord, F. F. *J. Am. Chem. Soc.* **1942**, *63*, 2745.

(13) Henglein, A.; Ershov, B. G.; Malow, M. *J. Phys. Chem.* **1995**, *99*, 14129.

(14) Wang, Z. L.; Ahmadi, T. S.; El-Sayed, M. A. *Surf. Sci.* **1997**, *380*, 302.